

1 **Primary spinel+chlorite inclusions in mantle garnet formed at**
2 **ultrahigh-pressure**

3

4 **Marcello Campione^{1*}, Simone Tumiati², and Nadia Malaspina¹**

5

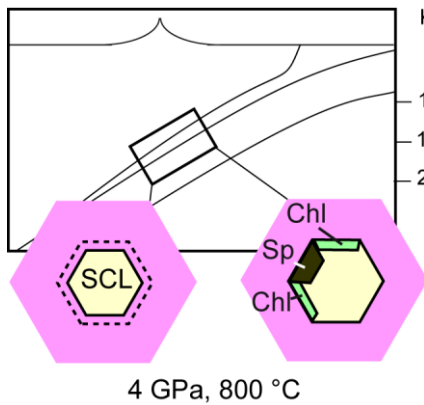
6 1. Department of Earth and Environmental Sciences, Università degli Studi di Milano Bicocca,
7 Piazza della Scienza 4, I-20126 Milano, Italy

8 * Corresponding author (email: marcello.campione@unimib.it)

9 2. Department of Earth Sciences, Università degli Studi di Milano, Via Botticelli 23, I-20133
10 Milano, Italy

11

12 ABSTRACT



Km Multiphase inclusions represent microenvironments where the
100 interaction between fluid and host mineral is preserved during
150 the rock geological path. Under its peculiar chemical-physical
200 constraints, the entrapped solute-rich fluid might follow a
crystallisation mechanism which is not predictable through
simple equilibrium arguments. In this letter, by modelling of

19 solid-solution equilibrium and the application of principles of mass conservation, we demonstrate
20 that cavities in mantle garnet filled with slab-derived fluids can re-equilibrate to
21 pyrope+spinel+chlorite assemblage at the same high P-T of their formation. The basis of this
22 occurrence is a dissolution-reprecipitation mechanism, triggered by a dilute, non-equilibrated slab
23 fluid.

24

25 **Introduction**

26 Primary inclusions (fluid or solid multiphase) in mantle minerals represent the remnant of the fluid
27 phase produced by dehydration reactions in the subducted slab and subsequently equilibrated with
28 the overlying supra-subduction mantle peridotites. Natural and experimental studies demonstrated
29 that saline aqueous inclusions with variable solute load prevail in high pressure (HP) rocks
30 (Scambelluri and Philippot, 2001; Touret, 2001), whereas multiphase solid inclusions in some
31 ultrahigh pressure (UHP) rocks have been attributed to silicate-rich fluids or hydrous melts at
32 supercritical conditions, namely supercritical liquids (Bureau and Keppler, 1999; Carswell and van
33 Roermund, 2005; Ferrando *et al.*, 2005; Korsakov and Hermann, 2006; Malaspina *et al.*, 2006;
34 Stöckhert *et al.*, 2001). These inclusions are frequently hosted by minerals stable at mantle depths,
35 such as garnet, and show the same textural features as fluid inclusions (Frezzotti and Ferrando,
36 2015; Fig. 1). The mineral infillings of the solid multiphase inclusions are generally assumed to
37 have crystallised by a simultaneous precipitation from the solute load of dense supercritical liquids
38 equilibrating with the host rock. Moreover, the occurrence of phases stable at UHP, such as coesite
39 or microdiamond, has long been considered evidence of precipitation from such liquids at pressure
40 above 3 GPa. Here, we demonstrate that even a mineral association characterised by phases usually
41 considered stable at relatively low pressure in mantle system (*e.g.* spinel + chlorite), would
42 potentially crystallise at UHP by chemical fluid/host interaction.

43 We will consider as a case study a well-known example of multiphase solid inclusions occurring in
44 the cores of garnets forming orthopyroxenites from the Maowu Ultramafic Complex (Eastern
45 China), interpreted as hybrid rocks resulting by the interaction of previous harzburgites and slab-
46 derived silica-rich liquids ($P = 4$ GPa, $T = 800$ °C) at the slab-mantle interface (Chen *et al.*, 2017;
47 Malaspina *et al.*, 2006). These multiphase inclusions have negative crystal shapes and constant
48 volume proportions of the mineral infillings consisting of spinel \pm orthopyroxene, and hydrous
49 phases gedrite/pargasite, chlorite, phlogopite, \pm talc, \pm apatite (Malaspina *et al.*, 2006, 2015; Fig. 1).

50 Some inclusions still preserve liquid water at the interface between mineral infillings and the cavity
51 wall (Malaspina *et al.*, 2017). Recently, Malaspina *et al.* (2015) demonstrated the epitaxial
52 relationship between spinel and garnet (Fig. 1A) which suggested nucleation of spinel under near-
53 to-equilibrium conditions. On the contrary, hydrous phases (amphiboles, chlorite and \pm talc
54 \pm phlogopite) nucleate in a non-registered manner and likely under far-from-equilibrium conditions.
55 The epitaxial growth of spinel with respect to garnet and the ring-shaped chlorite + water
56 assemblage filling the space between the host garnet and the other inclusion minerals (Malaspina *et*
57 *al.*, 2017), suggest that spinel and chlorite formed at UHP together with the garnet cores. However,
58 from a thermodynamic point of view, spinel should never be stable in a chemical system
59 characterised by pyrope + H₂O, at any P-T range (Fig. 2). Surprisingly, in nature we can count a
60 number of examples where spinel occurs in garnet-hosted primary diamond-bearing (hence UHP)
61 multiphase inclusions from Bardane, Ugelvik and Svartberget in the Western Gneiss Region
62 (Carswell and van Roermund, 2005; Malaspina *et al.*, 2010; Scambelluri *et al.*, 2010; van
63 Roermund, 2009; van Roermund and Drury, 1998; Van Roermund *et al.*, 2002; Vrijmoed *et al.*,
64 2008, 2006). We will show how this occurrence is driven by a dissolution-reprecipitation
65 mechanism triggered by precise constraints on the composition of the supercritical liquid phase
66 released by the slab.

67

68 **Results**

69 Multiphase solid inclusions in garnet represent the heritage of a series of processes comprising: i)
70 formation of the cavity, and ii) crystallisation of the solute within the cavity. The determined
71 morphological and compositional features of the solid phases can be exploited in order to gain
72 insights into the dynamics of these processes. Among the identified solid phases within
73 microcavities in garnet, spinel occupies a distinctive position (Fig. 1). The reasons for that derives
74 from the following characteristics, which were already evidenced by (Malaspina *et al.*, 2015): i)

75 spinel is not present in all the cavities, ii) spinel is the only (anhydrous) oxide phase when present,
76 iii) spinel is the only epitaxial phase with garnet when present. On the basis of these characteristics,
77 spinel was attributed a role of nucleation initiator for the solid phases occupying the cavity. Here,
78 we obtain deeper insights into the crystallization mechanism by the analysis of solution-solid
79 equilibrium in a model MgO-Al₂O₃-SiO₂-H₂O (MASH) system and the application of principles of
80 mass conservation.

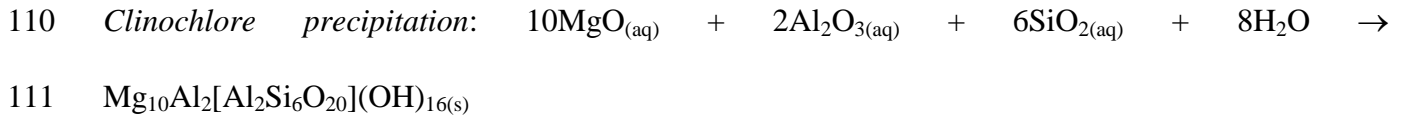
81 If aqueous fluids released by the slab are under the condition to equilibrate with solid phases, their
82 molal composition would be close to 0.11, 0.18, and 3.7, in terms of dissolved MgO, Al₂O₃, and
83 SiO₂ components, in accordance with the experimental composition of the fluid phase in
84 equilibrium with a K-free eclogite at 4 GPa and 800 °C (Kessel *et al.*, 2005, Fig. 3). This means that
85 the water released by the dehydration of slab minerals might enrich by significant amounts of the
86 sole silica component, as far as its path is sufficiently long before the slab-mantle interface is
87 reached. The effects of such fluids on the peridotite layer at the slab-mantle interface might be
88 distinguished as follows: i) if in contact with a pure water fluid, the minerals of the peridotite layer
89 might undergo dissolution. Dissolution might be negligible if the transition of fluids is fast and
90 alternated by periods of dry conditions. On the contrary, dissolution might persist if the fluid is
91 entrapped in cavities. ii) If in contact with a silica-rich fluid, the forsteritic component of the
92 peridotite layer might react with the fluid, giving rise to a pyroxene-rich layer, according to the
93 reaction $\text{Mg}_2\text{SiO}_4 + \text{SiO}_{2(\text{aq})} = \text{Mg}_2\text{Si}_2\text{O}_6$, acting as a "filter".

94 At a late stage of process ii), the fluid escaping the pyroxene-rich filter might be at a composition in
95 equilibrium with the mantle peridotite, namely 5.3, 0.31, and 3.0 in terms of MgO, Al₂O₃, and SiO₂
96 molalities (Dvir *et al.*, 2011, Fig. 3).

97 As far as process i) is concerned, one should evaluate if a subsequent event of dissolution-
98 reprecipitation within pyrope cavities might bring about an equilibration of the fluid-solid system at
99 the same P-T conditions of its formation. In order to demonstrate this evolution of the cavity, we
100 must perform a hypothesis on the precipitating phases. On the basis of the assessed composition of

101 our multiphase inclusions in pyrope-rich garnet (Malaspina *et al.*, 2015), it is clear that spinel and
 102 clinochlore can be reasonably considered the products of this precipitation, since stable assemblage
 103 pyrope-spinel-clinocllore occurs only at $P \geq 4$ GPa, and forsterite, corundum, Mg-staurolite, and
 104 coesite are never present within the cavity (Fig. S1). Hence, the cavity should contain, at
 105 equilibrium, spinel and clinochlore as phases nucleated on pyrope after its dissolution, [leaving a](#)
 106 [fluid with a composition in equilibrium with the pyrope-spinel-clinocllore assemblage.](#)

107 Pertinent chemical equations read:



112
 113 If one refers to 1 kg H_2O , the mass balance of the whole process reads:

114 $M = m + 3p_y - s_p - 10c_l$

115 $A = a + p_y - s_p - 2c_l$

116 $S = s + 3p_y - 6c_l$

117 $H = 56 - 8c_l$

118 Where M , A , and S (m , a , and s) are the final (initial) molalities of MgO , Al_2O_3 , and SiO_2 of the
 119 fluid entrapped in the cavity, H are the moles of free water, p_y , s_p , and c_l are the moles of
 120 congruently dissolved pyrope, precipitated spinel, and precipitated clinochlore, respectively. The
 121 solution of this system of equations gives:

122
$$p_y = \frac{A-a}{2} + \frac{2(S-s)}{3} - \frac{M-m}{2}$$

123
$$s_p = \frac{S-s}{3} - (A-a)$$

124
$$c_l = \frac{A-a}{4} + \frac{S-s}{6} - \frac{M-m}{4}$$

125 The constrain of positive values for p_y , s_p , and c_l allows us to define the space of the m , a , and s
 126 parameters, which determine the composition of the slab-derived fluid when the composition of the
 127 fluid in equilibrium with the pyrope-spinel-clinochlore assemblage is known. Such fluid was
 128 calculated to have a composition of $M = 0.15$, $A = 0.0096$, and $S = 0.12$ (Supplementary
 129 Information, Fig. 3B). These concentrations appear reliable if compared with the 0.13 molal
 130 experimental congruent solubility of garnet grossular (Fockenberg *et al.*, 2008). For our purposes,
 131 we consider the fluid in equilibrium with the pyrope-spinel-clinochlore assemblage to have
 132 concentrations within the intervals $M = 0.15 \div 0.39$, $A = 0.0096 \div 0.13$, and $S = 0.12 \div 0.39$, which give

133
$$p_y = (0.01 \div 0.13) - \frac{a}{2} - \frac{2s}{3} + \frac{m}{2}, \quad s_p = (0.0 \div 0.030) + a - \frac{s}{3}, \quad c_l = (-0.015 \div 0) - \frac{a}{4} - \frac{s}{6} + \frac{m}{4}. \quad A$$

134 trivial upper limit of initial molalities is $m = M$, $a = A$, and $s = S$, which zero the first member of the
 135 equations, whereas the lowest limit of pure water ($m = a = s = 0$) is admitted. Since the m term is
 136 positive in each equation, the mass balance gives no constrain on the upper limit of m and, while c_l
 137 increases with m , s_p is independent of m . On the contrary, a silica-rich fluid as that in equilibrium
 138 with the slab ($m = 0.11$, $a = 0.18$, $s = 3.7$) would give rise to negative p_y , s_p , and c_l .

139 By way of example, consider a fluid with composition $m = 0.20$, $a = 0$, and $s = 0$. Under such
 140 hypothesis the roots are $p_y = 0.11 \div 0.23$, $s_p = 0 \div 0.030$, and $c_l = 0.035 \div 0.050$ (H undergoes a
 141 decrement of $0.5 \div 0.7\%$, which gives rise to a negligible correction of the previous molalities). By
 142 scaling these results on the volume of a typical cavity ($10^4 \mu\text{m}^3$), considering that the molar volume
 143 of water is $14 \text{ cm}^3 \text{ mol}^{-1}$ at 4 GPa and 800 °C (Zhang and Duan, 2005), the moles of pyrope
 144 dissolved in the cavity and the moles of precipitated spinel and clinochlore are $(1.4 \div 2.9) \times 10^{-12}$,
 145 $(0 \div 3.8) \times 10^{-13}$, and $(4.5 \div 6.4) \times 10^{-13}$, respectively. Assuming a molar volume of 110, 40 and 1100
 146 $\text{cm}^3 \text{ mol}^{-1}$ for pyrope, spinel, and clinochlore, respectively, the dissolved volume of pyrope results

147 150±300 μm³, whereas the volume of precipitated spinel is 0±15 μm³ and that of clinocllore is
148 500±700 μm³. All these volume predictions are consistent to what observed in nature (Fig. 1).

149

150 **Conclusions**

151 The systematic presence of spinel+chlorite inclusions in many subduction zone mantle peridotites
152 reflects a slab-mantle interface characterised by the transit of dilute aqueous fluids which may
153 consist of pure H₂O. These fluids are non-equilibrated fluids released by the slab minerals having
154 the attitude to dissolve garnet (Fig. 4). If slab-derived fluids are SiO₂-enriched (Fig. 3), they will
155 react with the overlying mantle peridotites forming orthopyroxenite layers (grey zone in Fig. 4).
156 Once entrapped in the metasomatic-forming garnet (stage 1 in Fig. 4), they can dissolve it and bring
157 the system to an equilibrium state of py-sp-cl assemblage (Fig. S1) through a dissolution-
158 reprecipitation mechanism (stage 2 in Fig. 4). The subsequent retrograde path undergone by the
159 inclusion-bearing rock triggers the crystallisation of the other hydrous phases (gedrite, phlogopite,
160 pargasite, talc), leaving an eventual residue of water solution (stage 3 in Fig. 4). On the light of the
161 drawn conclusions, spinel-chlorite bearing multiphase inclusions can be considered as witnesses of
162 crystallization processes at UHP. The fingerprint of such processes is sometimes revealed by a
163 “surprising” composition which, if analysed by sole equilibrium arguments, would lead to wrong
164 inferences about their formation history.

165

166 **Acknowledgements**

167 N. M. and S. T. thank the Italian Ministry of Education, University and Research (MIUR) [PRIN-
168 2012R33ECR]. S. T. thanks the Deep Carbon Observatory (DCO) for financial support.

169

170

171

172 **References**

- 173 Bureau, H., Keppler, H. (1999) Complete miscibility between silicate melts and hydrous fluids in
174 the upper mantle : experimental evidence and geochemical implications. *Earth and Planetary*
175 *Science Letters* 165, 187–196.
- 176 Carswell, D. a., van Roermund, H.L.M. (2005) On multi-phase mineral inclusions associated with
177 microdiamond formation in mantle-derived peridotite lens at Bardane on Fjærtoft, west
178 Norway. *European Journal of Mineralogy* 17, 31–42.
- 179 Chen, Y., Su, B., Chu, Z. (2017) Modification of an ancient subcontinental lithospheric mantle by
180 continental subduction: Insight from the Maowu garnet peridotites in the Dabie UHP belt,
181 eastern China. *Lithos* 278–281, 54–71.
- 182 Connolly, A.D. (1990) Algorithm based on generalized thermodynamics. *American Journal of*
183 *Science* 290, 666–718.
- 184 [Dvir, O., Pettke, T., Fumagalli, P., Kessel, R. \(2011\) Fluids in the peridotite–water system up to 6](#)
185 [GPa and 800 °C: new experimental constraints on dehydration reactions. *Contributions to*](#)
186 [Mineralogy and Petrology](#) 161, 829–844.
- 187 Ferrando, S., Frezzotti, M.L., Dallai, L., Compagnoni, R. (2005) Multiphase solid inclusions in
188 UHP rocks (Su-Lu, China): Remnants of supercritical silicate-rich aqueous fluids released
189 during continental subduction. *Chemical Geology* 223, 68–81.
- 190 [Fockenberg, T., Burchard, M., Maresch, W. \(2008\) The solubility of natural grossular-rich garnet in](#)
191 [pure water at high pressures and temperatures. *European Journal of Mineralogy* 20, 845–855.](#)
- 192 Frezzotti, M.L., Ferrando, S. (2015) The chemical behavior of fluids released during deep
193 subduction based on fluid inclusions. *American Mineralogist* 100, 352–377.
- 194 [Kessel, R., Ulmer, P., Pettke, T., Schmidt, M. W., Thompson, A. B. \(2005\) The water–basalt](#)
195 [system at 4 to 6 GPa: Phase relations and second critical endpoint in a K-free eclogite at 700](#)
196 [to 1400 °C. *Earth and Planetary Science Letters* 237, 873–892.](#)

- 197 Korsakov, A. V., Hermann, J. (2006) Silicate and carbonate melt inclusions associated with
198 diamonds in deeply subducted carbonate rocks. *Earth and Planetary Science Letters* 241,
199 104–118.
- 200 Malaspina, N., Alvaro, M., Campione, M., Wilhelm, H., Nestola, F. (2015) Dynamics of mineral
201 crystallization from precipitated slab-derived fluid phase: first in situ synchrotron X-ray
202 measurements. *Contributions to Mineralogy and Petrology* 169, 26.
- 203 Malaspina, N., Hermann, J., Scambelluri, M., Compagnoni, R. (2006) Polyphase inclusions in
204 garnet–orthopyroxenite (Dabie Shan, China) as monitors for metasomatism and fluid-related
205 trace element transfer in subduction zone peridotite. *Earth and Planetary Science Letters* 249,
206 173–187.
- 207 Malaspina, N., Langenhorst, F., Tumiati, S., Campione, M., Frezzotti, M.L., Poli, S. (2017) The
208 redox budget of crust-derived fluid phases at the slab-mantle interface. *Geochimica et*
209 *Cosmochimica Acta* in press.
- 210 Malaspina, N., Scambelluri, M., Poli, S., Van Roermund, H.L.M., Langenhorst, F. (2010) The
211 oxidation state of mantle wedge majoritic garnet websterites metasomatised by C-bearing
212 subduction fluids. *Earth and Planetary Science Letters*, 417–426.
- 213 Scambelluri, M., Philippot, P. (2001) Deep fluids in subduction zones. *Lithos* 55, 213–227.
- 214 Scambelluri, M., Van Roermund, H.L.M., Pettke, T. (2010) Mantle wedge peridotites: Fossil
215 reservoirs of deep subduction zone processes. *Lithos* 120, 186–201.
- 216 Stöckhert, B., Duyster, J., Trepmann, C., Massonne, H., Sto, B. (2001) Microdiamond daughter
217 crystals precipitated from supercritical COH + silicate fluids included in garnet , Erzgebirge ,
218 Germany. *Geology* 29, 391–394.
- 219 Sverjensky, D.A., Harrison, B., Azzolini, D. (2014) Water in the deep Earth: The dielectric constant
220 and the solubilities of quartz and corundum to 60 kb and 1200 °C. *Geochimica et*
221 *Cosmochimica Acta* 129, 125–145.
- 222 Touret, J.L. (2001) Fluids in metamorphic rocks. *Lithos* 55, 1–25.

223 van Roermund, H.L.M. (2009) Mantle-wedge garnet peridotites from the northernmost ultra-high
224 pressure domain of the Western Gneiss Region, SW Norway. *European Journal of*
225 *Mineralogy* 21, 1085–1096.

226 van Roermund, H.L.M., Drury, M.R. (1998) Ultra- high pressure ($P > 6$ GPa) garnet peridotites in
227 Western Norway: exhumation of mantle rocks from > 185 km depth. *Terra Nova* 10, 295–
228 301.

229 van Roermund, H.L.M., Carswell, D., Drury, M.R., Heijboer, T.C. (2002) Microdiamonds in a
230 megacrystic garnet websterite pod from Bardane on the island of Fjørtoft, western Norway:
231 evidence for diamond formation in mantle rocks during. *Geology* 30, 959–962.

232 Vrijmoed, J., Smith, D., van Roermund, H.L.M. (2008) Raman confirmation of microdiamond in
233 the Svartberget Fe- Ti type garnet peridotite, Western Gneiss Region, Western Norway.
234 *Terra Nova* 20, 295–301.

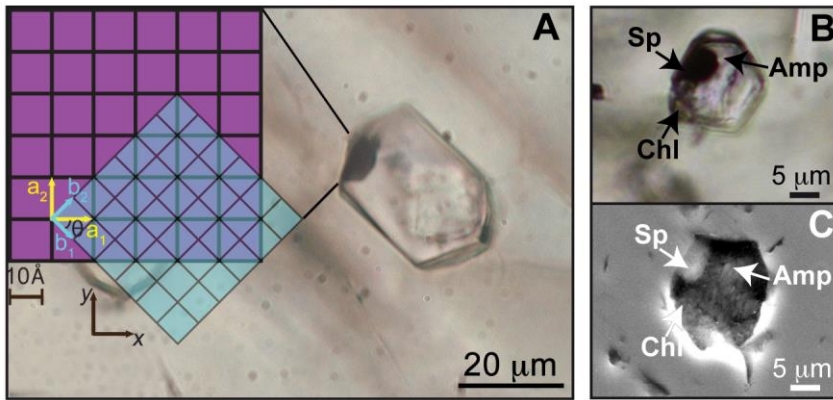
235 Vrijmoed, J.C., van Roermund, H.L.M., Davies, G.R. (2006) Evidence for diamond-grade ultra-
236 high pressure metamorphism and fluid interaction in the Svartberget Fe–Ti garnet peridotite–
237 websterite body, Western Gneiss Region, Norway. *Mineralogy and Petrology* 88, 381–405.

238 Zhang, Z., Duan, Z. (2005) Prediction of the PVT properties of water over wide range of
239 temperatures and pressures from molecular dynamics simulation. *Physics of the Earth and*
240 *Planetary Interiors* 149, 335–354.

241

242

243 **Figure 1**

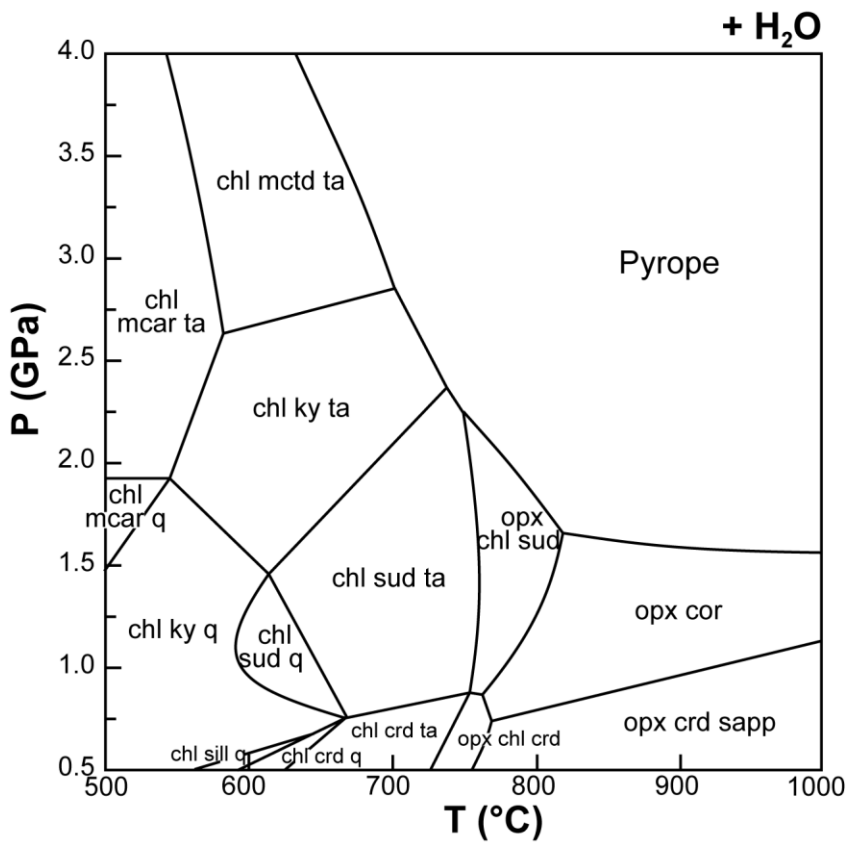


244

245 **Figure 1** A) Photomicrograph of a multiphase solid inclusion in metasomatic garnet from
246 Maowu Ultramafic Complex (Dabie Shan, China). Inset represents the relative orientation of the
247 spinel {100} surface lattice (light blue) with respect to the garnet {100} surface lattice (violet) for
248 the coincidence at $\theta = -45^\circ$ (from Malaspina *et al.*, 2015); B, C) Negative-crystal shaped
249 multiphase solid inclusion (plane polarised transmitted light and Secondary Electron image) with
250 evident microstructural relations between spinel, chlorite and amphibole (gedrite).

251

252 **Figure 2**

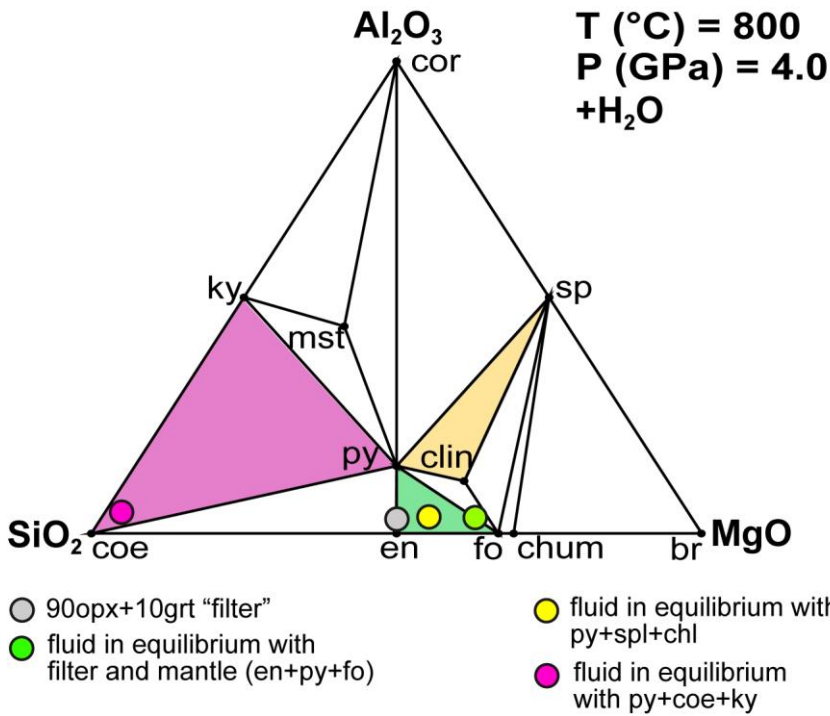


253

254 **Figure 2** Predicted P-T stability fields for mineral assemblages in the simplified system MgO
255 (3 mol) - SiO₂ (3 mol) - Al₂O₃ (1 mol) + H₂O calculated with Perple_X software package
256 (Connolly, 1990). Mineral abbreviations: chl=chlorite, mctd=Mg-clorithoid, ta=talc, mcar=Mg-
257 carpholite, ky=kyanite, q=quartz, opx=orthopyroxene, sud=sudoite, cor=corundum, sill=sillimanite,
258 crd=cordierite, sapp=sapphirine.

259

260 **Figure 3**

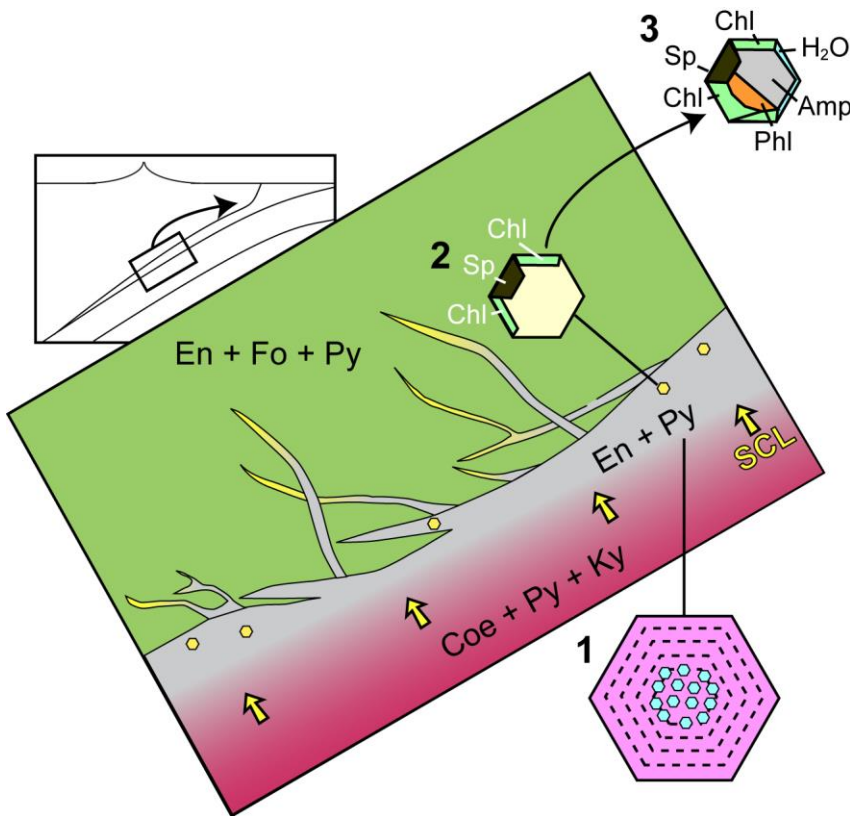


261

262 **Figure 3** Chemographic projection of a water-saturated MgO-Al₂O₃-SiO₂ system at 4 GPa and
 263 800 °C, showing stable assemblages of coe-ky-py, py-en-fo, and py-sp-clin. **Experimental**
 264 equilibrium slab fluid compositions and mantle fluid compositions are indicated by purple and
 265 green dots, respectively. **Calculated** compositions of a fluid in equilibrium with py-sp-chl
 266 assemblage is indicated by yellow dot. The composition of the orthopyroxenite containing
 267 multiphase inclusions in garnet is indicated by a grey dot. Mineral abbreviations same as in Figure 2
 268 and coe=coesite, mst=Mg-staurolite, py=pyrope, en=enstatite, clin=clinocllore, sp=spinel,
 269 fo=forsterite, chum=clinohumite, br=brucite.

270

271 **Figure 4**



272

273 **Figure 4** Schematic cartoon showing aqueous fluid entrapped by growing metasomatic garnet
274 (1) after the interaction of slab-derived supercritical liquid (SCL) and the supra-subduction mantle
275 peridotite forming garnet orthopyroxenite (grey layer and veins). Light blue hexagons represent
276 primary aqueous inclusions in pyrope. Garnet/fluid interaction yields to a dissolution and
277 precipitation process that triggers epitaxial nucleation of spinel and chlorite during garnet growing
278 at UHP (2). Subsequent post-entrapment crystallisation of the other hydrous phases such as gedrite,
279 phlogopite, pargasite and talc during retrograde P-T path (3) leaves an eventual residue of water
280 solution (light blue rim). Modified after Malaspina *et al.* (2017).

281

282 **Primary spinel+chlorite inclusions in mantle garnet formed at**
283 **ultrahigh-pressure**

284

285

286 **Marcello Campione¹, Simone Tumati², and Nadia Malaspina^{1*}**

287

288 1. Department of Earth and Environmental Sciences, Università degli Studi di Milano Bicocca,
289 Piazza della Scienza 4, I-20126 Milano, Italy

290 * Corresponding author (email: nadia.malaspina@unimib.it)

291 2. Department of Earth Sciences, Università degli Studi di Milano,
292 Via Botticelli 23, I-20133 Milano, Italy

293

294 **Supplementary Information**

295

296 **Thermodynamic modelling.** The P–T isochemical section of Figure 2 was calculated by Gibbs free
297 energy gridded minimisation with the software Perple_X (Connolly, 2005), considering a fixed bulk
298 composition corresponding to pure pyrope ($\text{Mg}_3\text{Al}_2\text{Si}_3\text{O}_{12}$) at H_2O -saturated conditions. We used
299 the thermodynamic database and equation of state for H_2O of Holland and Powell (1998).

300 The compatibility diagrams of Figure 3 and Figure S1 were calculated with the software Perple_X
301 in the MASH system ($\text{MgO}-\text{Al}_2\text{O}_3-\text{SiO}_2-\text{H}_2\text{O}$), projected from H_2O .

302 MgO , Al_2O_3 and SiO_2 dissolved in water in equilibrium with py+coe+ky (pink in Figure 3),
303 en+fo+py (green in Figure 3), and py+cl+sp (yellow in Figure 3) were calculated using the aqueous
304 speciation-solubility code EQ3 (Wolery, 1992) adapted to include equilibrium constants calculated
305 with the Deep Earth Water (DEW) model (Facq *et al.*, 2014; Sverjensky *et al.*, 2014). The results

306 of such calculations are reported in the following tables for comparison with experimental
307 solubilities found in literature:

308

Equilibrium slab-fluid	
DEW-EQ3 (py-coe-ky assemblage)	EXP (Kessel et al. 2005) pink dot in Fig. 3
0.017	0.11
0.0037	0.18
1.77	3.7

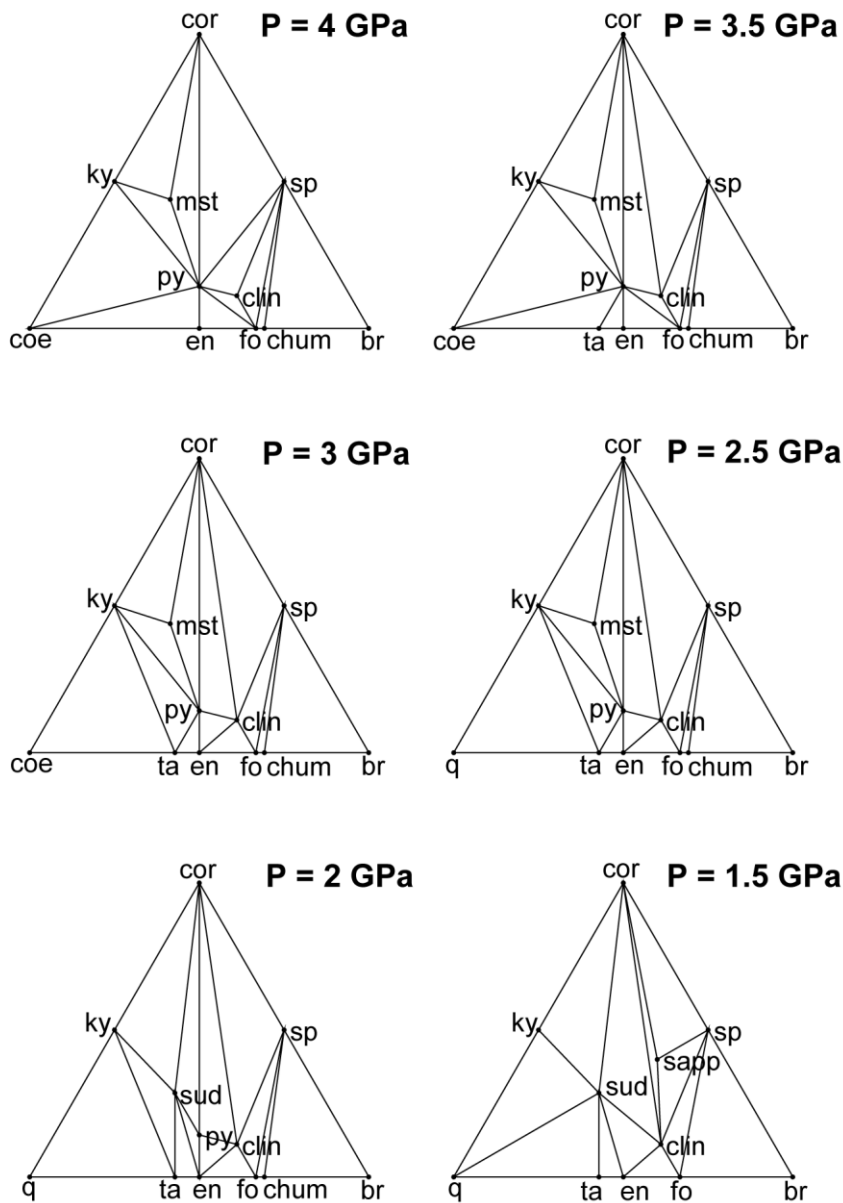
309

Equilibrium mantle-fluid	
DEW-EQ3 (en-fo-py assemblage)	EXP (Dvir et al. 2011) green dot in Fig. 3
0.25	5.29
0.0026	0.31
0.20	3.0

310

Fluid in equilibrium with py-sp-cl assemblage	
DEW-EQ3	EXP (Fockenberg et al. 2008) yellow dot in Fig. 3
0.15	0.39
0.0096	0.13
0.12	0.39

311



312

313 **Figure S1** Compatibility diagrams of water-saturated MgO-Al₂O₃-SiO₂-H₂O system at 800 °C
 314 and 1.5–4 GPa, projected from H₂O, showing that the stable assemblage pyrope-spinel-clinocllore
 315 occurs only at UHP conditions. Mineral abbreviations same as Figures 2 and 3 of the manuscript.

316

317 **Supplementary References**

318 Connolly, J.A.D. (2005) Computation of phase equilibria by linear programming: A tool for
 319 geodynamic modeling and its application to subduction zone decarbonation. *Earth and*
 320 *Planetary Science Letters* 236, 524–541.

- 321 Facq, S., Daniel, I., Montagnac, G., Cardon, H., Sverjensky, D.A. (2014) In situ Raman study and
322 thermodynamic model of aqueous carbonate speciation in equilibrium with aragonite under
323 subduction zone conditions. *Geochimica et Cosmochimica Acta* 132, 375–390.
- 324 Holland, T.J.B., Powell, R. (1998) An internally consistent thermodynamic data set for phases of
325 petrologic interest. *Journal of Metamorphic Geology* 16, 309–43.
- 326 Wolery, T.J. (1992) EQ3/6, A Software Package for Geochemical Modeling of Aqueous Systems:
327 Package Overview and Installation Guide (Version 7.0). Lawrence Livermore National
328 Laboratory, Livermore, California.